Operability of a Natural Gas-Air Rotating Detonation Engine

Ian V. Walters*, Christopher L. Journell*, Aaron Lemcherfi†, Rohan M. Gejji†, Stephen D. Heister‡, and Carson D. Slabaugh§

Purdue University School of Aeronautics and Astronautics, West Lafayette, IN 47907

A combustor was developed to operate with natural gas and air as the primary propellants at elevated chamber pressures and air preheat temperatures representative of land based power generation gas turbine engines. Detonation dynamics were studied to characterize the operability of rotating detonation based pressure gain combustion systems for this application. Measurements of chamber wave dynamics were performed using high-frequency pressure transducers and high speed imaging of broadband combustion chemiluminescence. The rotating detonation engine was tested with two injector configurations across a broad range of mass flux ($200 - 500\ kg/m^2/s$)**, equivalence ratio** ($0.85 - 1.2$)**, and oxygen mass fraction** ($23.2 - 35\%$) **conditions to determine the effect of operating parameters on the propagation of detonation waves in the combustor. Wave propagation speeds of up to 70% of the mixture Chapman-Jouguet detonation velocity and chamber pressure fluctuations greater than 4 times the mean chamber pressure were observed. Supplementing the air with additional oxygen, varying the equivalence ratio, and enriching the fuel with hydrogen revealed that combustor operability is sensitive to the chemical kinetics of the propellant mixture. Comparing the operational trends of the two injector configurations suggests that one design mixes the incoming propellants more effectively. While most test conditions exhibited counter-rotating detonation waves within the chamber, the injector design with superior mixing characteristics was able to support single wave propagation.**

*Graduate Student, School of Aeronautics and Astronautics, AIAA Student Member.

†Research Engineer, School of Aeronautics and Astronautics, AIAA Member.

‡Raisbeck Distinguished Professor, School of Aeronautics and Astronautics, AIAA Fellow.

§Assistant Professor, School of Aeronautics and Astronautics, AIAA Senior Member.

Nomenclature

CR	=	backpressure nozzle contraction area ratio
PGC	=	pressure gain combustion
$RDWC$	=	rotating detonation wave combustor
G	=	mass flux, $kg/m^2/s$
P_c	=	mean chamber pressure, MPa
P'	=	mean chamber pressure fluctuation amplitude, MPa
T_3	=	combustor inlet temperature, K
$Y_{O_2}^{Ox}$	=	mass fraction of oxygen in oxidizer
$Y_{H_2}^{F}$	=	mass fraction of hydrogen in fuel
λ	=	detonation cell size
ϕ	=	equivalence ratio

I. Introduction

Modern gas turbine engines are the result of decades of incremental technology development, resulting in few remaining opportunities for step-changes in engine performance. Development and adoption of pressure-gain combustion (PGC) systems provides a promising avenue for achieving this desired performance increase. State-of-the-art systems use constant pressure, deflagrative combustion, which results in a total pressure loss due to non-isentropic effects. A PGC device realizes a cycle-averaged total pressure increase by an unsteady combustion process where gas expansion is constrained during heat addition [1]. This results in a more efficient thermodynamic cycle as it produces greater energy availability for the same heat release [2, 3]. Detonation based combustion systems provide one method of attaining PGC because the chemical reactions occur faster than surrounding gas expansion. The timescale disparity results in combustion that is constrained and occurs at near-constant volume conditions. A detonation is also capable of providing higher rates of heat release because it propagates at velocities several orders of magnitude higher than a deflagration. Engine concepts that leverage these advantages will realize systems-level benefits via smaller combustors, in addition to efficiency gains.

The rotating detonation wave combustor (RDWC) configuration shows significant promise for realizing detonation-based PGC. In an RDWC, detonation waves are formed by a single deflagration-to-detonation transition during engine startup via direct initiation or by natural azimuthal instabilities in the combustor [4, 5]. One or more detonation waves then propagate transverse to the flow of incoming reactants, typically in an annular chamber. The configuration permits

a quasi-steady flow device, where incoming reactants are naturally valved by high pressures behind the detonation wave. The RDWC features a conventional feed system that relies on high injection pressure drops or fluidic valving (temporary cessation of injection due to the high pressure waveform) to permit operation at frequencies of order 1-10 kHz for airbreathing combustors. The quasi-steady flow due to high cycle frequencies and annular geometry eases integration with continuous flow turbomachinery systems and permits reuse of existing engine architectures.

Recent research has considered application of the RDWC to a range of propulsion systems, including turbojets, high speed air-breathing combustors, and rockets [5–11]. However, these studies are typically conducted at laboratory-scale conditions and with propellant combinations that readily detonate, such as hydrogen or ethylene with air or methane with oxygen. There has been comparatively less investigation of RDWCs for land based power generation applications, where the poor detonability of the common propellant combination, natural gas and air, presents unique challenges.

Several researchers have recently worked to demonstrate RDWC operation with less detonable propellants relevant to power generation systems. Bykovskii [12–14] conducted an extensive study of airbreathing RDWC operation with syngas mixtures, with specific emphasis on combustor scaling . Further work with their 500 mm RDWC studied methane-hydrogen mixtures at pressures up to 1.5 MPa and found that hydrogen fractions greater than $Y^F_{H_2} = 30\%$ supported operation with continuous spinning detonation waves. However, decreasing the hydrogen content to $Y^F_{H_2} = 16\%$ resulted in waves propagating in both directions, referred to as a "Continuous Multifront Detonation," while further decreases resulted in external combustion. Roy *et al.* [15, 16] similarly studied natural gas-hydrogen airbreathing RDWC operation in a 150 mm combustor, but found it was only able to support detonation with $Y^F_{H_2} > 85\%$. While preheating the air to 480 K and operating at above-atmospheric chamber pressures of 0.3 MPa produced more robust operation, it failed to expand the range of operable natural gas concentrations. This was attributed to significant increases in the chemical induction time and thereby detonation cell size as the natural gas concentration increased, until the cells outgrew their combustor hardware scale. Given the limited scope of present research, there is a need to investigate operation of an RDWC with natural gas-air propellants at combustion chamber conditions relevant to land based power generation ($p_c = 1 - 2\ MPa,\ T_3 = 600 - 800\ K$) to explore the potential for this application.

Key obstacles to the realization of RDWC cycle benefits include nonideal detonation propagation, dynamic injection, unsteady mixing, and parasitic loss mechanisms. Development of design methodologies for scaling combustors from laboratory flow conditions and propellants to those found in gas turbine engines for power generation is currently intractable due to the nonlinear coupling between the injection fluid mechanics and reaction chemistry, which is highly sensitive to the geometry of the combustion device. It is therefore necessary to study RDWC systems with reactants and combustor operating conditions representative of this application, where demonstrating operation has remained challenging. The present study seeks to understand how the dynamic injection, mixing, and chemical kinetic processes that occur in RDWCs affect engine operation for the reactants and flow conditions of land-based power generation gas turbines. A combustor was developed to study detonation wave dynamics using a combination of integral and

time-resolved techniques. Operability of the device was tested with natural gas and air propellants, chamber pressures up to 2 MPa, and air preheat temperatures up to 800 K.

II. Experiment Description

A. RDWC Test Article

A combustor was developed to demonstrate and investigate RDWC operation with natural gas and air propellants. The RDWC is designed to operate with a mean chamber pressure up to 2 MPa and permits variation of propellant flowrates, stoichiometry, propellant types, system backpressure, and air pre-heat temperature up to 800 K. The combustor geometry is depicted in the cross sectional view of Fig. 1. The combustion chamber outside diameter is 228 mm, the annular gap is 19 mm, and the length is 130 mm. The combustor was tested with two distinct injector designs. In both configurations, the oxidizer is fed axially through a slot at the head end of the chamber, while fuel is injected from orifices downstream of the oxidizer throat. Further details of the injection system are discussed in Section II.C.

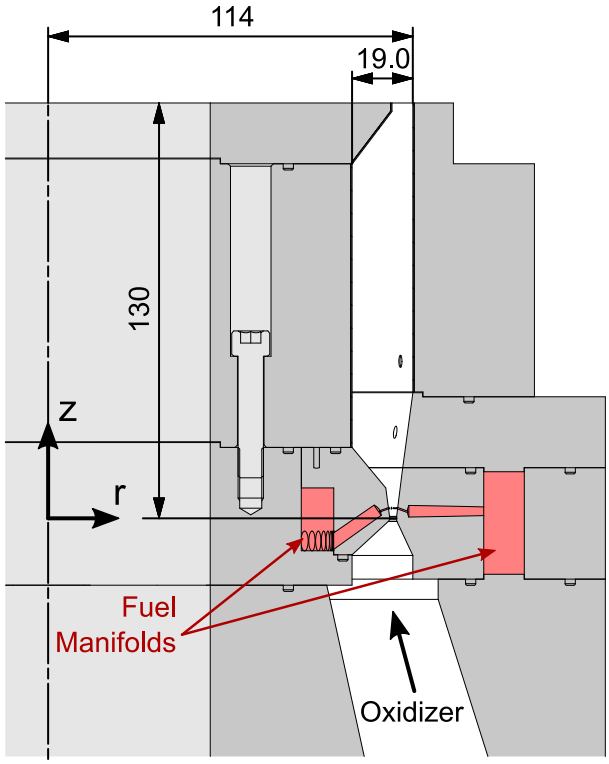

Fig. 1 Cross section of RDWC test article with major dimensions labeled (in mm).

A thrust stand with requisite propellant supply systems was installed at the Maurice J. Zucrow Laboratories [17, 18] to provide a test platform for the combustor. The test platform can supply up to 10 kg/s of non-vitiated, heated air to the test article with commensurate flows of natural gas, gaseous oxygen, nitrogen, cooling water, and other gaseous fuels. Oxygen can be independently injected into the air flow to increase the mass fraction of oxygen in the oxidizer flow,

$Y_{O_2}^{Ox}$, from 23.2% (air) to 40%. Increasing the oxygen content of the oxidizer can be necessary to increase the range of operability for less detonable propellants. Natural gas is sourced from a local pipeline, while oxygen and other gaseous fuels are supplied by manifolds of high-purity cylinders. The natural gas composition is taken as a monthly average of the mole fraction of major species reported by the distributor (CH_4 92.4%, C_2H_6 6%, N_2 1%, CO_2 0.3%, C_3H_8 0.3%) [19].

The mass flow rates of fuel and oxidizer are metered by critical flow venturi nozzles (CFVNs) that conform to ISO specifications [20]. Upstream pressure and temperature are monitored throughout each test to compute mass flow rates. The pressure ratio across each CFVN is typically high enough to maintain a choked condition, but a throat pressure tap is also installed to CFVNs at risk of unchoking to permit calculation of mass flow rates at all conditions. The thermophysical properties of all fluids were computed using the NIST Reference Fluid Thermodynamic and Transport Properties Database (REFPROP) [21]. This permits a fully real-gas treatment for computation of mass flow rates, acoustic velocities, and other thermodynamic data. Natural gas was treated as a mixture of the above constituents for both flowrate and stoichiometry calculations.

Uncertainty of mass flow rates, and subsequently operating conditions, are computed using the Kline-McClintock method of uncertainty propagation [22]. Error analysis included precision and bias of flow measurements, as well as uncertainty of natural gas composition, CFVN throat diameter, computed CFVN discharge coefficient, and critical flow function. Total uncertainty of each mass flow rate is approximately 0.8% with a 95% confidence interval. This results in a typical uncertainty in operating conditions of 0.5% of mass flux, 0.9% of equivalence ratio, and 0.1% of mass fraction of oxygen in the main oxidizer flow.

A pre-detonator device generates a detonation wave which is injected into the chamber and initiates combustion of the main propellants [23]. The pre-detonator feeds hydrogen and oxygen through a 4.6 mm tube closed at its head end by a spark plug. Spark discharge initiates a combustion front which then transitions to a detonation wave via a Shchelkin spiral integral to the tube wall. After a short, chaotic transient, limit-cycle operation establishes with one or more rotating detonation heads in the main combustor. Propellant flows are established prior to ignition to reduce transient effects of valve actuation, regulator response, and manifold priming. Combustion is terminated by replacing the fuel flow with an inert gas purge. Without active cooling measures, the test duration is limited to approximately 1 s because of the high thermal power density.

B. Cell Size Analysis

The propellant combination of natural gas-air presents unique challenges for use in an RDWC because the primary fuel constituent, methane, is difficult to detonate due to slow combustion kinetics that result in a large detonation cell size. As shown in Fig. 2, the detonation cell size of methane, denoted λ, is approximately 300 mm at atmospheric pressure and temperature. The detonation cell size has been widely used in RDWC preliminary design and interpretation

of test results, where common heuristic design guidelines dictate that the cell size serves as a minimum characteristic dimension of an RDWC chamber [5, 7, 16, 24]. However, cell sizes are based on measurements of detonation propagation through perfectly premixed reactants with idealized boundary conditions, while a detonation in an RDWC propagates through highly turbulent reactants with strong mixture fraction gradients and ill-defined boundary conditions. It is then unclear whether cell-forming transverse waves exist in an RDWC. As a result, their role in supporting propagation of the detonation front and the applicability of the cell size as a scaling parameter is not apparent.

Despite the differences in flow physics and boundary conditions between canonical configurations and RDWCs, several experiments have observed trends in combustor operability with cell size [7, 16, 24], which suggests that application of the cell size may still provide insight as an approximate scaling parameter. Prior studies in detonation channels have shown that the transverse waves in a cellular detonation front facilitate propagation of unstable detonations [25, 26]. The complex flow field found in RDWCs will inevitably produce an unstable detonation, which suggests that the transverse waves may still play a role. With this view of the detonation cell size as an approximate scaling parameter, it remains clear that a natural gas-air combustor requires operation at high pressures and temperatures to permit reasonably sized hardware.

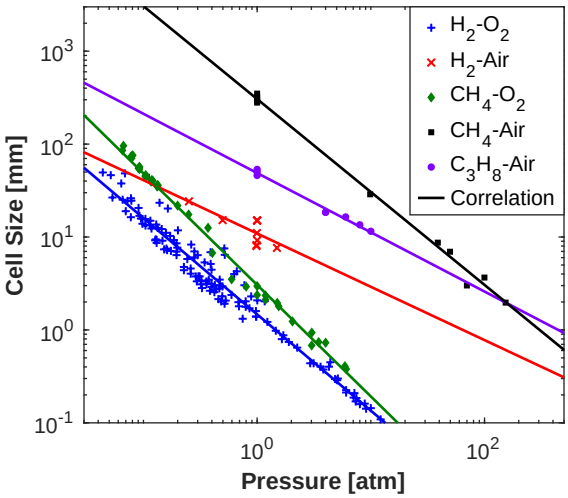

Fig. 2 Detonation cell size data for several propellant combinations showing variation with respect to pressure for constant temperature and mixture fraction.

A correlation was developed to estimate the cell size dependence on pressure, temperature, and oxygen mass fraction using available data for the methane-oxygen-nitrogen system [27–30]. The correlation facilitates combustor sizing and will subsequently be used to investigate the importance of detonation cell size on RDWC operation. The correlation is given as

$$\lambda = (3.05\text{mm}) \exp\left(\frac{2\beta}{1.219 + 0.11\beta}\right) \left(\frac{P}{1\text{atm}}\right)^{\frac{\beta - 22.56}{18.8}} \left(\frac{T}{300\text{K}}\right)^{-1}, \tag{1}$$

where β is the number of moles of nitrogen per mole of oxygen in the mixture ($\beta = 3.76$ for air), while P and T are the initial pressure and temperature of the mixture. The functional form of Eq. 1 is based on trends observed in detailed calculations of induction lengths [31]. The correlation was developed with the view that the detonation cell size is most appropriate as a heuristic parameter in the design and analysis of RDWCs. As a result, no attempt was made to correct for factors that differ between the original experiments used to measure cell size and the present application to RDWCs, such as the presence of wall curvature, lateral relief, turbulence, and flow stratification. The green and black lines of Fig. 2 show the cell size computed by Eq. 1 for $\beta = 0$ and $\beta = 3.76$, respectively. A least squares fit was used to compute the remaining lines. The targeted range of operating conditions with chamber pressures of 1-2 MPa and the oxidizer preheated to 600 K produces an estimated cell size of 8 to 15 mm.

This analysis of detonation cell sizes does not account for the minor constituents in natural gas, such as ethane and propane. However, it has been shown that these additional species serve to sensitize the mixture via contribution of H radicals in initial chain branching reactions [32]. The addition of 5% ethane can reduce the ignition delay time by a factor of two. This effect will help to reduce the cell size and thereby increase the operable range of the RDWC.

The cell size analysis was used to inform the baseline dimensions of the combustor. The radial gap was selected to be on the order of one to two cell widths at the target operating conditions. The chamber diameter was then selected to ensure a minimum 10:1 ratio to the radial gap. This ratio was selected to reduce the influence of curvature effects while maintaining a tractable combustor size. A large chamber diameter to radial gap ratio has been shown to produce significant radial variations in the detonation structure [33].

C. Injector Design

Two distinct injector concepts were designed and tested to evaluate their impact on combustor operability. The injection system of an RDWC must produce mixing on spatiotemporal timescales that sufficiently prepare the reactant mixture prior to the periodic arrival of detonation wavefronts. In addition, combustor operation and performance is highly sensitive to the geometric details of the injection system. A key parameter is the location of fuel injection relative to the throat of the oxidizer system, which has a significant impact on the injection dynamics and subsequent mixing. A brief review of airbreathing RDWC injector designs in the public literature showed that most operable systems placed the fuel injection downstream of the air injection throat [4, 7–9, 12, 15, 34–36]. Injecting fuel downstream of the oxidizer throat may make the dynamic injection and flow recovery process more receptive to coupling with the dynamics of the chamber environment, which may play a role in supporting stable operation. In contrast, RDWCs that operate with rocket propellants have been shown to produce stable operation with injection upstream or downstream of the oxidizer throat [5]. The distinction could be explained by operational differences between airbreathing and rocket RDWCs, including the relative strength of the detonation wave. Without the additional nitrogen in air, a detonation wave in a rocket RDWC will propagate faster and produce higher peak pressures. The pressure waves are then sufficiently

strong to travel upstream past the oxidizer throat and perturb the fuel injection processes. Given this distinction between RDWC systems, the current design places fuel injection downstream of the air throat.

Figure 3 presents detailed schematics of both an axial and sting injector design, respectively denoted A and B. Both designs inject fuel from orifices in the expansion region of a circumferentially continuous oxidizer injection slot, forming a jet-in-crossflow. The location of fuel injection orifices was selected to promote interaction between unsteady shock trains from both the fuel and air. The shock train location will vary widely in response to the dynamic pressure from each passing detonation wave. The principle difference between the two injector designs is that injector B has two axial oxidizer injection slots. While design A injects fuel from both the inner and outer circumference of the combustion chamber, design B injects fuel from the middle of the combustion channel into both axial air slots. Both concepts attempt to distribute fuel injection across the cross section of incoming oxidizer flow to increase the fraction of oxidizer exposed to the fuel. The area ratio between the combustion chamber and oxidizer throat is 8.6 for injector A and 9.4 for injector B.

Two different nozzle contraction ratios (CR), 1.93 and 2.75, were tested with each injector configuration. This alters the Mach number of propellant flows within the chamber and the pressure ratio from each propellant manifold into the chamber. The injector dynamic response and the mixing near the head end of the chamber between detonation wave fronts is changed dramatically, particularly as the oxidizer injection is changed from a choked to unchoked condition. Changing backpressure nozzles varied the pressure ratio across the air injection slot from 1.5 - 2.5 while it changed from 2.5 - 4 across the fuel injection orifices. The pressure ratios were selected such that the injectors could respond after being checked off by each detonation head in time to sufficiently fill and mix propellants. Variation of combustor backpressure also affects the fill height, which is the axial extent of propellant inflow to the chamber between wave passage. Based on the approximation that premixed reactants fill the chamber head end volumetrically at the mean chamber pressure, the fill height is estimated to vary between 20-40% of the chamber length downstream of the injector throat due to changing backpressure nozzles.

D. Instrumentation and Optical Diagnostics

Operation of the experiment is remotely monitored and controlled using a National Instruments (NI) based data acquisition and control system (DACS). The NI signal conditioning hardware records analog inputs from pressure transducers, thermocouples, valve position indicators, and thrust stand load cells using a 16 bit ADC (NI PXIe-6375). It also provides digital control for valve actuation and analog set-point control of electronic regulators for closed-loop feedback control of pressure upstream of CFVNs (Tescom ER5000). A NI LabView Virtual Instrument (VI) is used for experiment operation and data acquisition. The VI provides auto-sequenced control with redline monitoring for automatic abort of test operations. All experiment control and condition monitoring operates at a frequency of 1 kHz [17]. High-frequency pressure and timing measurements were recorded with an independent NI data acquisition system

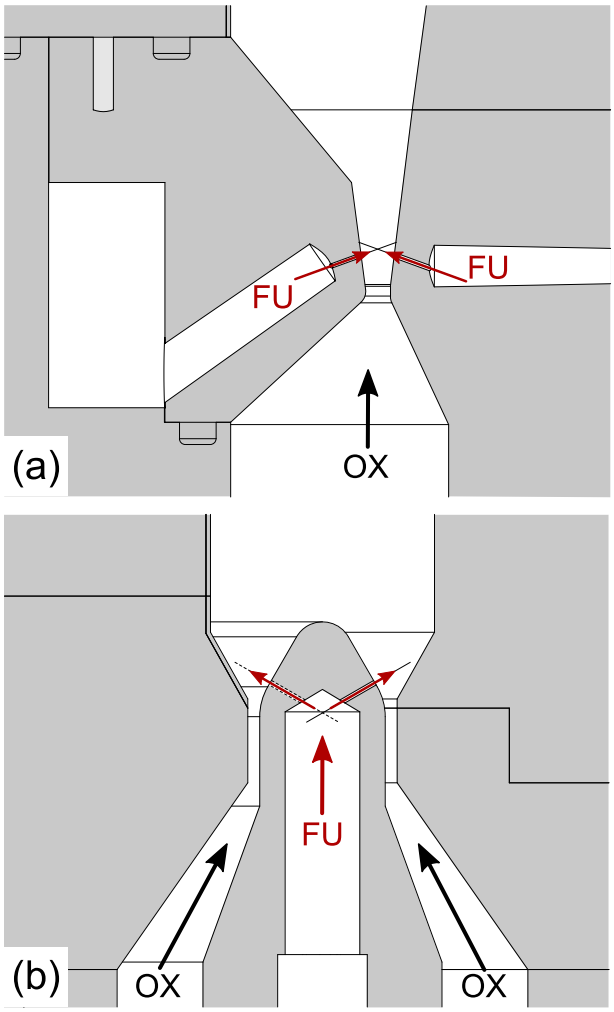

Fig. 3 Detailed schematic of combustor head end geometry for axial injector A (a) and sting injector B (b) with arrows highlighting the flow of fuel (FU) and oxidizer (OX).

that provides non-multiplexed readout on up to 32 channels at frequencies up to 2 MHz.

The RDWC is instrumented with an array of low-and high-frequency pressure transducers within the combustion chamber and propellant manifolds. A pressure transducer in the Capillary Tube Attenuated Pressure (CTAP) configuration with a length-to-diameter ratio of approximately 2000 was included for comparison to other studies. Pressure fluctuations were measured with water cooled piezoresistive transducers (Kulite WCT312M), which have a reported element natural frequency of 1.65 MHz. Prior studies have shown that it is difficult for transducers to survive in the preferred, flush-mount configuration due to the high heat fluxes associated with high pressure detonative combustion [5, 37]. Therefore, the transducers are installed in a recessed cavity with a resonant frequency > 50 kHz, which provides a measurement of detonation pressure with lower amplitude attenuation and phase lag than a comparable semi-infinite tube pressure installation while protecting the instrument [38]. The transducer outputs were recorded at 1 MHz to provide a high level of temporal resolution. While much consideration was given to the selection and installation of

transducers for pressure measurements, the inherent limitations of pressure measurements in an RDE restricts their quantitative interpretation. The installation approach required for the high-frequency pressure transducers biases their measurements, while the interpretation of mean pressures from low-frequency transducers is unclear given that RDEs are a fundamentally unsteady system. As a result, the collected pressure measurements are primarily used to provide directional sensitivities and are not considered to be an accurate measurement of the thermodynamic state within the combustion chamber. Figure 4 specifies instrument port locations in the combustion chamber and propellant manifolds, while Table 1 lists the coordinates of each port. Reported measurements refer to the instrumentation port number to specify transducer location. Chamber transducers CC-01 and CC-02 were installed in all tests to allow consistent comparison across test days and instrumentation configurations.

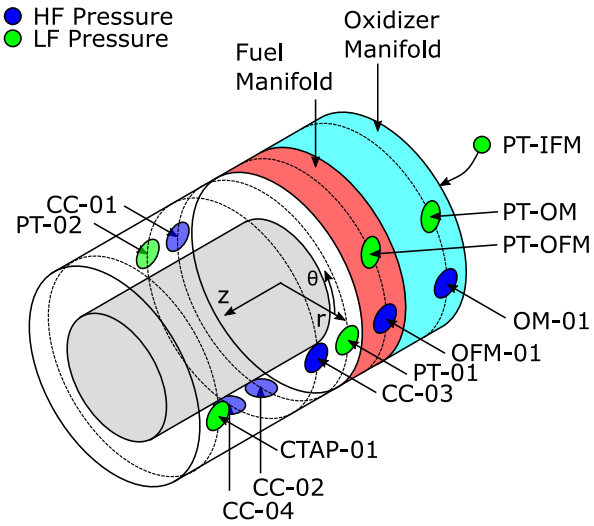

Fig. 4 Measurement port locations around circumference of combustor.

Table 1 Coordinates of transducer port locations on combustor.

Port	Location	θ [deg]	z [mm]
OM-01	Oxidizer Manifold	0	-41
OFM-01	Outer Fuel Manifold	0	-2
CC-01	Chamber	180	27
CC-02	Chamber	270	27
CC-03	Chamber	0	49
CC-04	Chamber	270	49
PT-OM	Oxidizer Manifold		
PT-OFM	Outer Fuel Manifold		
PT-IFM	Inner Fuel Manifold		
PT-01	Chamber	0	27
PT-02	Chamber	180	49
CTAP-01	Chamber	270	100

The wave dynamics in the chamber are visualized by direct imaging of the combustor annulus. Images are recorded at 110 kHz at a resolution of 384 x 384. Broadband chemiluminescence from the chamber is collected by a 500 mm focal-length, f/5.6 objective lens (Nikon AF-S 200-500mm) and imaged by a Phantom v2512 high speed CMOS camera. Chamber images provide information about the wave number, topology, and velocity.

III. Results and Discussion

The RDWC was tested with both injector configurations across a range of operating conditions in a broad parametric survey of mass flux, G, mass fraction of oxygen in the main oxidizer flow, $Y_{O_2}^{Ox}$, equivalence ratio, ϕ, and mass fraction of hydrogen in the fuel flow, $Y_{H_2}^{F}$. Approximately 60 tests were conducted with each injector, where half of all tests used air without oxygen enrichment. The range of tested conditions is summarized in Table 2.

Table 2 Range of tested combustor operating conditions.

$G\ [kg/m^2/s]$	ϕ	$Y_{O_2}^{Ox}$ [%]	T_3 [K]	$Y_{H_2}^{F}$ [%]	P_c [MPa]
200-500	0.85-1.2	23.2-35	575-800	0-17	0.7-1.8

A. Chamber Dynamics

Figure 5a presents a pressure-time history illustrating a typical test sequence. Propellant flows are established prior to ignition to allow fuel manifolds to fully prime. The pre-detonator injects a detonation wave into the chamber and ignites the main chamber propellants at t = 0. Ignition triggers a short startup transient where the number and direction of detonation heads can change on a per-cycle basis. The pressure fluctuations then enter a limit cycle characteristic of one or more rotating detonation waves within the chamber. The pressure-time history in Fig. 5b shows steep-fronted waveforms with modulating peaks that decay to approximately the mean chamber pressure. The pressure measurements

at CC-01 and CC-02 exhibit a consistent phase relationship, indicating the presence of co-rotating detonation waves in the chamber. Inspection of high speed video reveals a single wave circumscribing the chamber, corroborating observations from the pressure transducers. This test was conducted with injector B using the CR = 1.93 nozzle. The operating conditions were a mass flux of $G = 350 kg/m^2/s$, equivalence ratio of $\phi = 0.90$, air inlet temperature of $T_3 = 590K$, and pure air as the oxidizer. Operation with a single detonation wave was only observed at a narrow range of conditions similar to this test.

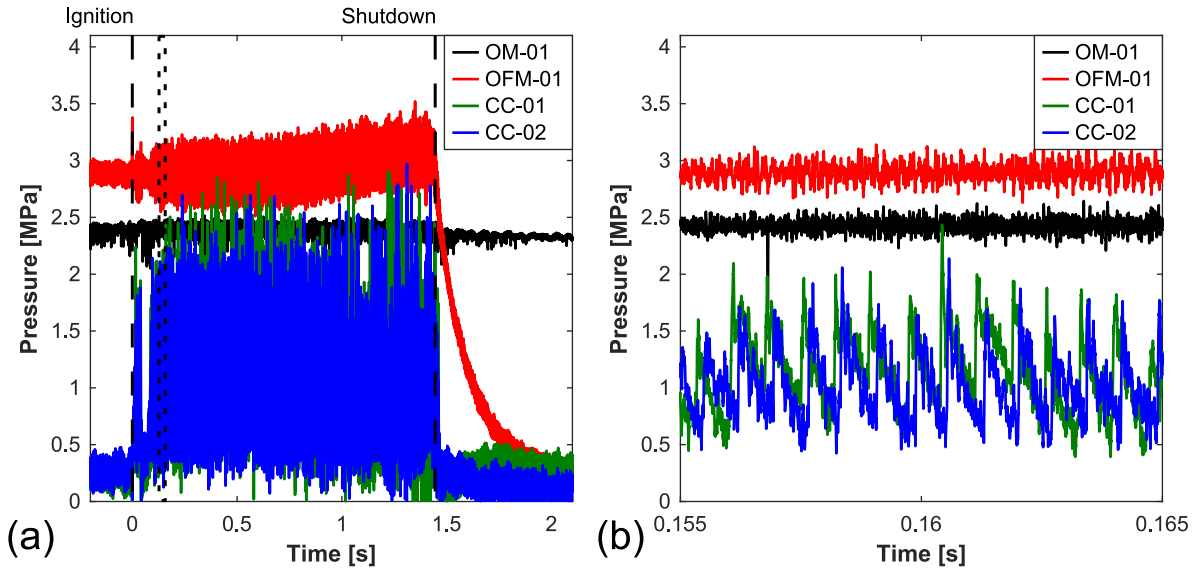

Fig. 5 Representative high frequency pressure measurements illustrating (a) test sequence and (b) steep fronted waves from a rotating detonation wave in the chamber.

Figure 6 shows the operating wave mode and velocity as a function of flow condition for the injector B and CR = 1.93 nozzle configuration. This was the only configuration to exhibit either single or co-rotating waves. Single-wave operation was observed at each of the three tested mass fluxes and only in a narrow range of equivalence ratios between 0.90 and 0.95. While most other conditions produced counter-rotating waves with one wave propagating in each direction, the test conducted at a mass flux of $G = 450 kg/m^2/s$ and equivalence ratio of $\phi = 1.0$ resulted in two waves propagating in each direction. Equivalence ratios greater than 1.15 resulted in steady combustion. The wave speed relative to the CJ velocity varied between 55-65% for all conditions operating with this injector and nozzle configuration.

The power spectral density (PSD) of the chamber pressure signal computed from a 100 ms window of the representative test is shown in Fig. 7a. The steep-fronted oscillations evident at measurement location CC-01 correspond to the fundamental frequency of 1.45 kHz and subsequent harmonics. Measurement location CC-02 shows a similar sequence of harmonics. Both chamber pressure transducers exhibit a minor peak at 1.24 kHz near the fundamental frequency. This corresponds with a counter-propagating wave which gains strength and subsequently decays during the 100 ms window of the PSD, though the dominant operational mode is still a single detonation.

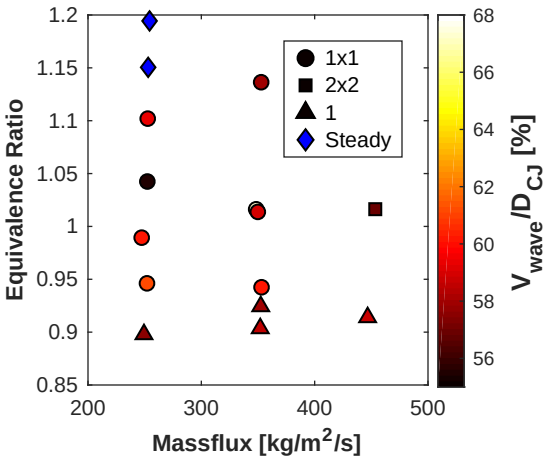

Fig. 6 Wave mode and velocity as a function of flow condition for injector B using the CR = 1.93 nozzle.

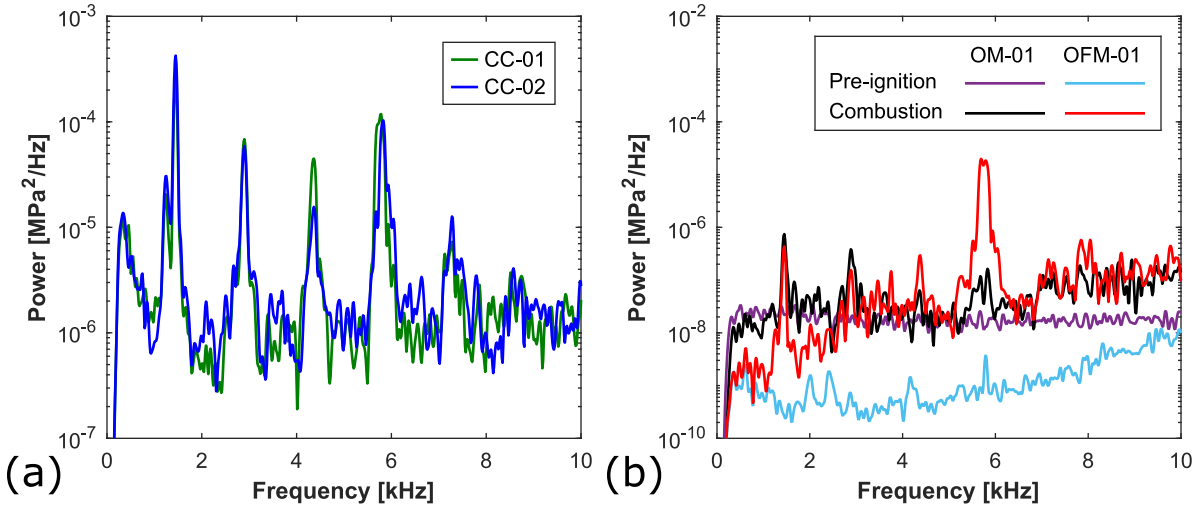

Fig. 7 Power spectral density plots of (a) chamber pressure transducers and (b) manifold pressure transducers.

The steep-fronted waves found in the combustion chamber apply forcing to the propellant manifolds. Spectral analysis of transducers located in the outer fuel and oxidizer manifolds, OFM-01 and OM-01 respectively, reveals periodic content in Fig. 7b. During combustion, both manifolds respond at the fundamental forcing frequency of 1.45 kHz, and higher harmonics. It is unclear why the fuel manifold responds so strongly at 5.8 kHz, the fourth harmonic of the chamber fundamental frequency. The peak frequency of both manifolds is observed to vary between harmonics of the chamber frequency across the range of tested conditions, though no trend is discernible. Figure 7b overlays a second PSD from a window immediately prior to ignition to see if any frequencies inherent to the manifolds persist. The oxidizer manifold exhibits no clear natural frequency, while the fuel manifold has natural resonances at 2 and 2.4 kHz. These manifold responses are typical of the parametric survey, where the forcing applied by steep-fronted detonation waves is observed in manifold pressure fluctuations, but there is no indication that the manifold acoustics correspond to

the chamber limit cycle frequency.

Imaging of the combustor annulus provides information about wave dynamics throughout each test. Figure 8a plots the time-history of pixel intensity around the chamber circumference by transposing the θ direction of Fig. 4 onto the y-axis, similar to the method of Bennewitz *et al.* [39]. Inspection of the pixel intensity time-history (referred to as the "detonation surface") reveals a single detonation wave propagating in the $+\theta$ direction, consistent with the phase relationship between CC-01 and CC-02 in Fig. 5. Comparison with the single image of Fig. 8b illustrates how the detonation surface can be used to extract information about the wave structure. The vertical width of lines on the detonation surface reflect the extent of post-wave combustion luminescence, seen extending from the wave front at $\theta = 85°$ to $\theta = 340°$ in Fig. 8b. An ideal detonation front would appear as a line of vanishing width in Fig. 8a. Changes in line slope and spacing make cycle-to-cycle variation in wave propagation apparent on the detonation surface, while it is difficult to ascertain from image sequences.

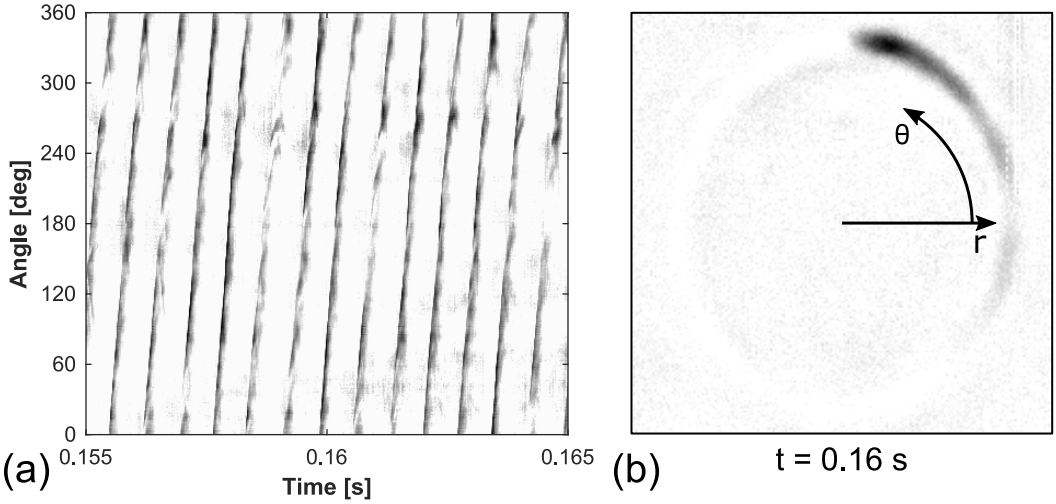

Fig. 8 Detonation surface plot (a) and high-speed image (b) showing a single detonation wave.

Figure 9 depicts the pressure-time history and detonation surface plot from another representative test with two counter-propagating detonation waves in the combustion chamber. This test was conducted with injector A and the CR = 2.75 nozzle, where the operating conditions were $G = 250 kg/m^2/s$, $\phi = 1$, $T_3 = 730K$, and pure air as the oxidizer. The wave intersection at $\theta = 0°$ and $\theta = 180°$ throughout the time slice of Fig. 9b is consistent throughout the duration of the test, aside from startup and shutdown transients. Transducer CC-01 is situated at the $\theta = 180°$ intersection point, resulting in the pressure fluctuation amplitudes seen in Fig. 9a that exceed three times the mean chamber pressure. Pressure probe CC-02 is located at $\theta = 270°$, resulting in lower fluctuation amplitudes and two peaks between each peak in CC-01. While the wave intersection points in this test are aligned with the inlets feeding the oxidizer manifold located upstream at $\theta = 0°$ and $\theta = 180°$, this is not observed at all operating conditions. The intersection points have been

observed to precess during the test while still producing high-amplitude pressure fluctuations at other flow conditions [40].

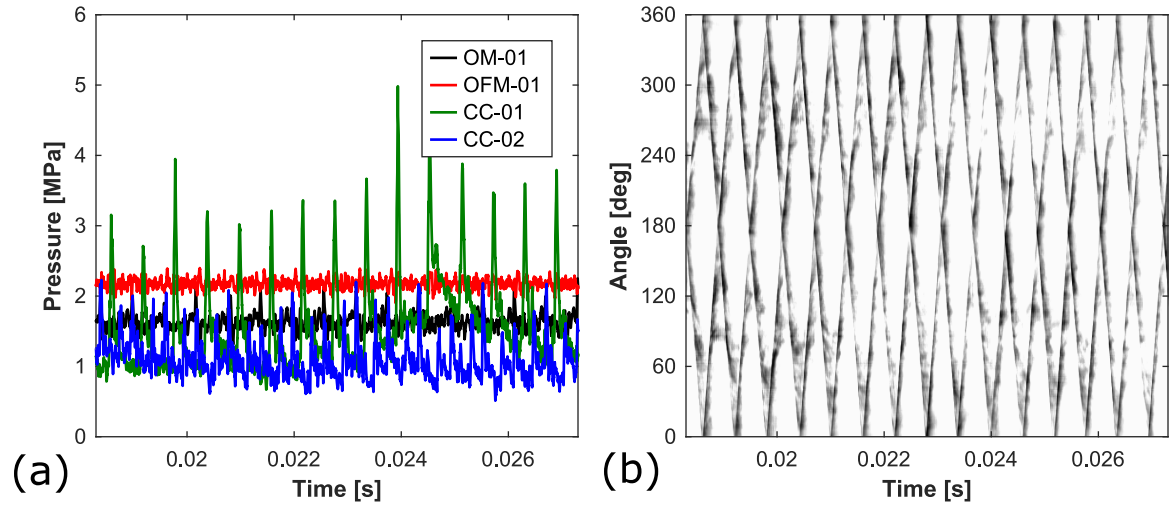

Fig. 9 Pressure time history (a) and detonation surface plot (b) for a representative test case with two counter-propagating detonation waves.

B. Analysis Approach

In order to understand the sensitivity of the strength and stability of chamber dynamics to operating condition, two metrics were selected to evaluate each test. The average amplitude of pressure fluctuations normalized by the mean chamber pressure measured with PT-02, P'/P_c, provides an indication of the strength of detonation waves in the chamber. The pressure fluctuation amplitude for a single transducer is computed as the difference between the mean peak pressure and mean valley pressure across a sufficient number of samples to converge the first-order moment [41].

Figure 10a and b illustrate the efficacy of the peak identification process for the pressure histories of Fig. 5b and Fig. 9a, respectively. The figure shows a plot of each pressure series notated with the identified peaks alongside a histogram of the pressure fluctuation amplitude for each transducer location. The overlapped histograms of Fig. 10 show that a single detonation wave produces a similar distribution of pressure fluctuation amplitudes at each transducer location. In comparison, Fig. 10b shows a test where the intersection point of counter-rotating waves aligned with a single transducer, producing peak pressures that do not appropriately characterize the overall chamber dynamics. There is little overlap in the distributions of pressure fluctuation amplitude for each transducer. A more representative value of P' is then obtained by averaging the pressure fluctuation amplitude measured across all installed transducers. The typical relative uncertainty of the normalized pressure fluctuation amplitude, P'/P_c, is 2-4% with a 95% confidence interval.

The coherence of wave dynamics was characterized by the fraction of spectral power contributing to the primary

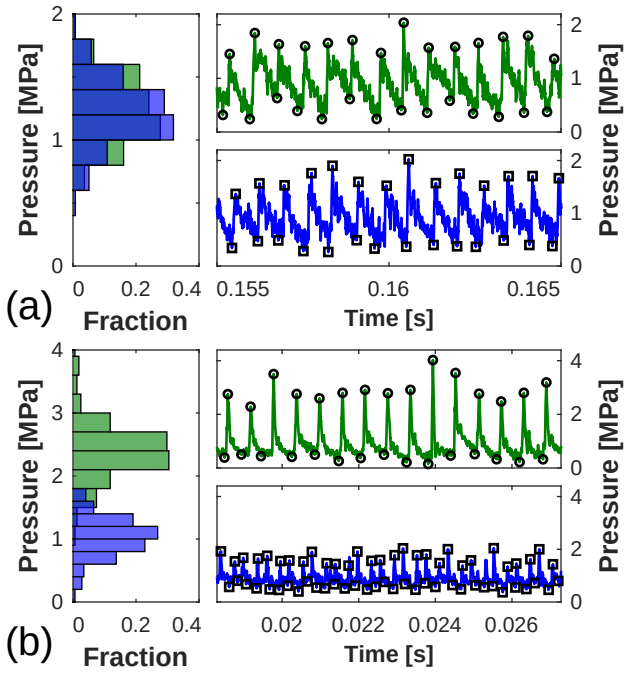

Fig. 10 Peak identification and distribution of pressure fluctuation amplitudes for representative test cases exhibiting (a) single and (b) counter-rotating wave modes.

limit-cycle process in the measured pressure-time history and was computed as the integral of the power spectral density under peaks corresponding to the fundamental frequency, harmonics, and subharmonics normalized by the total power contained in the signal. The domain of integration spanned until the power had dropped to 95% of the peak value, or an adjacent peak was found. Termed the power fraction (PF), this parameter is expected to approach unity for stable, robust chamber dynamics and will diminish to zero for weaker dynamics with additional frequencies that correspond to superimposed processes. Similar to the pressure fluctuation amplitude, the reported power fraction is an average of the power fractions computed for each installed pressure transducer.

Figure 11 demonstrates the ability of this method to distinguish signals affected by different types and magnitudes of contamination. Two synthetic signals are presented as examples, a sine wave and a periodic, steep-fronted waveform. Increasing the parameter σ systematically decreases the coherence of each signal using three corruption models. The "Noise" method adds white Gaussian noise with a variance of σ^2. The "Mix" model has been used in prior studies of signal regularity [42] and samples either the underlying signal or a uniformly distributed random value with probability σ. As σ increases, the corruption model transitions from sampling the true signal to sampling random noise. The sample timeseries use a value of $\sigma = 0.1$ for both the "Noise" and "Mix" models. Finally, the "Dephase" corruption method changes the signal phase by a random, uniformly distributed amount with probability σ, where a value of $\sigma = 0.02$ was selected for the plots of Fig. 11a.

Figure 11b then presents the power fraction computed for the six combinations of waveform type and corruption

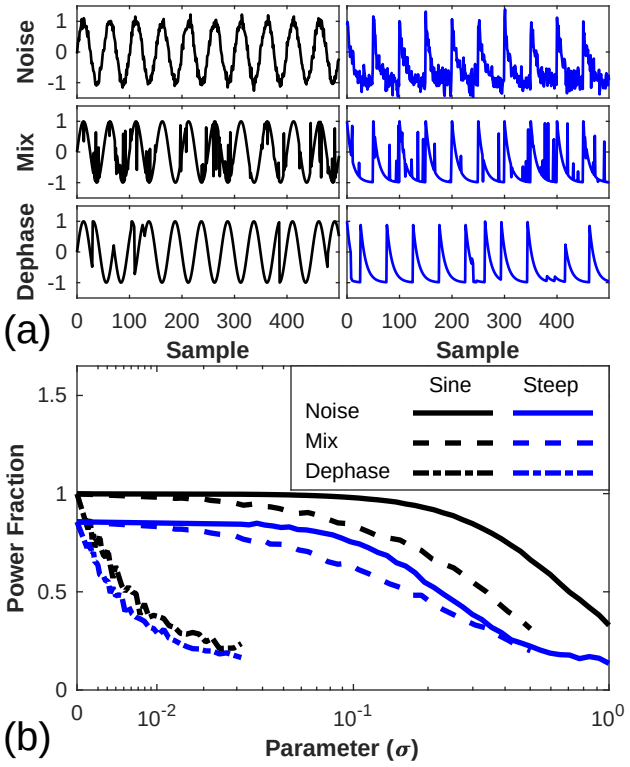

Fig. 11 Demonstration of power fraction metric with (a) synthetic sine wave and steep-fronted signals with three types of contamination and (b) power fraction for varying levels of signal contamination.

method over a range of the parameter value, σ. For each combination, the power fraction was averaged over 10-40 realizations of the corruption method. As expected, the power fraction of both the sine and steep-fronted waves begins near unity and is insensitive to the "Noise" and "Mix" corruption methods for $\sigma < 0.1$. Higher levels of contamination result in a gradual roll-off in power fraction. The "Dephase" corruption model results in a steep decline in power fraction for values of σ as low as 0.001. The high sensitivity to dephasing is the desired outcome, as it is most representative of the signal corruption that the power fraction attempts to differentiate.

The pressure fluctuation amplitude and power fraction are computed from a 100 ms window (150-600 waves, depending on operating condition) selected from the approximate middle of each test to avoid the transient effects of startup or fuel cutoff at shutdown. The pressure fluctuation amplitude was 1.9 and 2.4 for the two tests corresponding to Fig. 10a and b, respectively. The corresponding power fractions were 51% and 63%.

C. Global Operability

Figure 12 depicts scatter plots that summarize the range of tested conditions in terms of power fraction, estimated wave speed, and estimated cell size at mean chamber conditions. The markers are colored by the pressure fluctuation amplitude, while the shape indicates the injector configuration. Figure 12a shows that the power fraction, estimated wave velocity, and pressure fluctuation amplitude are all approximately correlated. This is expected, as faster detonation

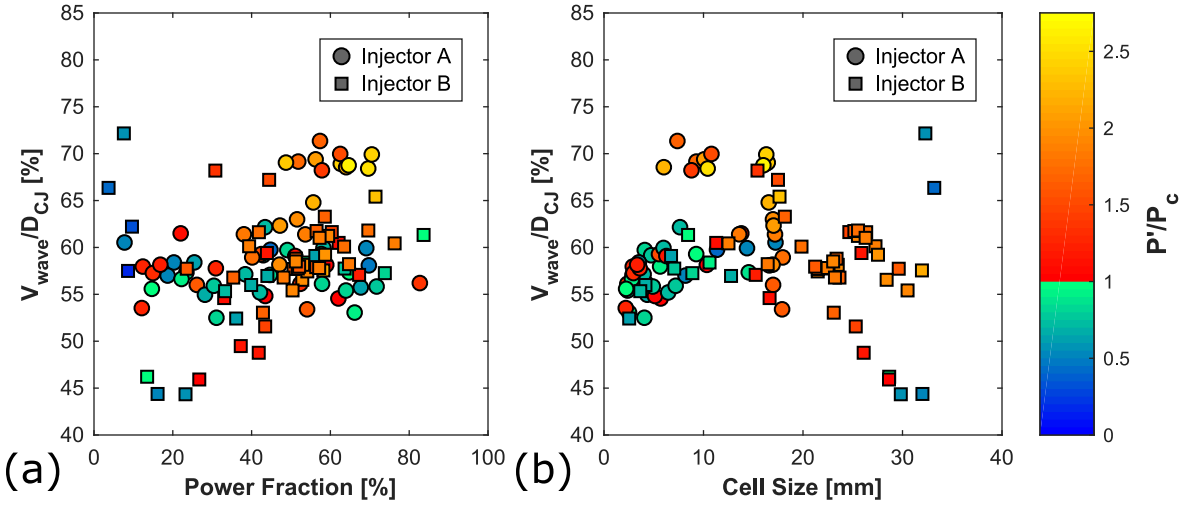

Fig. 12 Scatter plots of detonation quality evaluated by power fraction, pressure fluctuation amplitude, cell size, and estimated wave velocity.

waves will produce stronger leading shocks and thereby higher pressure fluctuations. Tests with high power fractions, indicating stable detonation propagation, will similarly tend to produce higher pressure fluctuation amplitudes because there are fewer auxiliary processes within the combustion chamber that could destructively interfere with and weaken the detonation.

Figures 12a also shows an approximate floor in the observed wave velocities between 50-60% of the CJ detonation velocity for the mixture. Studies of the deflagration-to-detonation transition process have found that deflagration waves will accelerate to approximately half of the CJ detonation velocity before spontaneous transition to detonation [26]. Furthermore, deflagration waves can propagate at this velocity in a quasi-steady manner, which produces an uncoupled precursor shock ahead of the combustion front wherein turbulence is likely the mechanism supporting self-propagation. This shock-turbulent reaction front complex has been modeled as a CJ deflagration, resulting in a predicted velocity that closely matches the observed 50% of the CJ detonation velocity [43]. In the present RDWC experiments, it is possible that the intense turbulence created in the inflow supports the propagation of a combustion wave similar to a CJ deflagration, which would explain the observed floor in velocity with moderate pressure fluctuation amplitudes.

Some of the points in Fig. 12a demonstrate the limitations of both the power fraction and the estimated wave velocity for interpretation of test outcome. For example, the two points at the upper left of the plot indicate tests that had estimated wave speeds of 65-75%. However, their low power fraction and pressure fluctuation amplitude indicates that these tests likely produced steady combustion instead of detonation waves. Test cases with high power fractions but very low pressure fluctuation amplitudes similarly resulted in steady deflagration. This highlights the benefit of using both the power fraction and pressure fluctuation amplitude when looking at trends between test cases.

Figure 12b compares the estimated wave speed and cell size with the pressure fluctuation amplitude. Here it is

apparent that the estimated cell size is not correlated with the pressure fluctuation amplitude or estimated wave speed. In fact, the cases with the highest pressure fluctuation amplitudes and wave speeds have cell widths that are approximately the width of the combustor or one half its width. As discussed in Section II.B, the nonideal flow field and boundary conditions found in an RDWC relegate the detonation cell size to an approximate scaling parameter. Figure 12b then suggests that the cell size must be of the right order of magnitude to support detonative operation, but that continued decreases do not guarantee more stable operation.

D. Parameter Sensitivities

The effect of individual inlet flow conditions on combustor operability was then investigated for each tested combination of injector and backpressure nozzle. The combustor mass flux, oxygen mass fraction, equivalence ratio, and hydrogen mass fraction were all varied independent of other operating conditions. Each test was conducted at either a high or low oxidizer inlet temperature, $T_3 = 710 - 750K$ and $T_3 = 600 - 675K$ respectively. Injector A could not be reliably ignited with the CR = 1.93 exit nozzle because of a high degree of flow expansion into the chamber. Pressure transducers at locations PT-01 and PT-02 measured approximately 70 kPa prior to ignition at this condition, while the oxidizer manifold pressure PT-OM was 1.3 MPa. This indicates the bulk velocity in the injection and combustion region was $O(800m/s)$ with a Mach number of 2.5, preventing the combustion process from occurring within the chamber.

Figure 13 shows the sensitivity of detonation propagation within the combustor to changes in the mass flux, G. These tests were conducted with unity equivalence ratio and an oxidizer inlet temperature, T_3, of $600 - 675K$. The mass fraction of oxygen in the oxidizer flow was fixed at $Y_{O_2}^{Ox} = 28\%$ with injector A, while pure air was used for the tests with injector B.

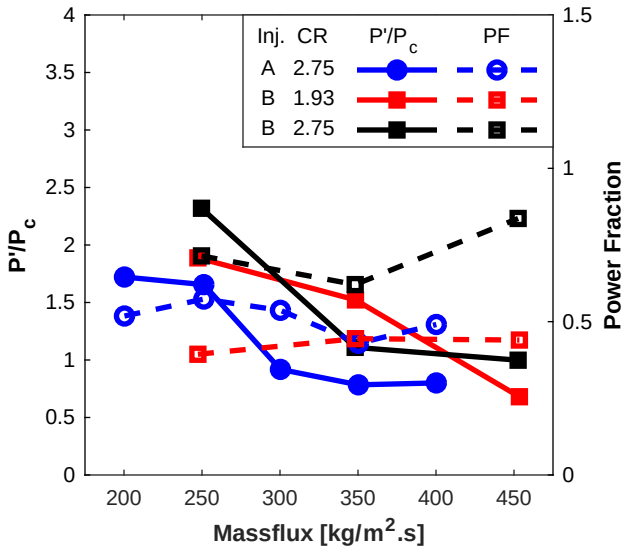

Fig. 13 Sensitivity of combustor operability with respect to mass flux, G.

The pressure fluctuation amplitude decreases with increasing mass flux for each combination of injector and backpressure nozzle. Similarly, power fraction decreases with increasing mass flux for injector A, consistent with detailed observations of the pressure-time history that indicate less stable wave propagation [40]. However, there is no clear trend in power fraction as the mass flux is increased for injector B with both backpressure nozzles. Inspection of the corresponding pressure-time histories shows that the pressure fluctuations are highly periodic, but low amplitude. In addition, the wave speed decreases from 65-70% of the CJ detonation velocity to 55-60%. This could correspond to a transition from low-order detonations to CJ deflagration waves. Increasing the mass flux also results in an increased number of detonation fronts in the combustor. For injector A, the number of waves increases from one propagating in each direction to two in each direction at $G = 300 kg/m^2/s$. Injector B with the CR = 2.75 nozzle behaves in the same manner, although the transition from one to two waves propagating in each direction is observed to occur at $G = 350 kg/m^2/s$ due to the more limited number of tested conditions. In contrast, Injector B with the CR = 1.93 nozzle maintains a single wave in each direction at $G = 350 kg/m^2/s$, but transitions to two waves in each direction by $G = 450 kg/m^2/s$. The number of waves within the chamber increases with mass flux for both injectors and results in a higher wave arrival frequency, which decreases the amount of time available to refresh the combustor channel with sufficiently mixed, fresh propellants. Combustion of reactants that are not completely mixed will then reduce the wave speed and pressure fluctuation amplitude, until a new equilibrium between wave strength and propellant mixing has been reached.

Variation of mass flux (Fig. 13) approximately isolates the effect of chamber pressure on the wave dynamics because the injection pressure ratios and Mach numbers remain constant for a given geometry defined by the combination of injector configuration and backpressure nozzle. The reduced pressure fluctuation amplitudes with increasing mass flux may then be a result of higher pressures suppressing the detonation waves. This is consistent with the observed operation of injector B with the CR = 1.93 nozzle, which produces a lower chamber pressure for a given mass flux and accordingly is able to operate at higher mass fluxes. Nozzles with high contraction ratios have also been shown to reflect the trailing oblique shock from the detonation front back into the injection region, which can adversely affect injection dynamics and lead to wave failure [44]. It should be noted that varying mass flux does not strictly isolate the effect of chamber pressure, as propellant mixing and chemical kinetics also depend on local gas thermophysical properties such as density.

Sensitivity to the chemical kinetic timescales of the propellant mixture was explored by changing the mass fraction of oxygen in the main oxidizer flow and the combustor inlet temperature while maintaining the equivalence ratio and mass flux constant at unity and $250 kg/m^2/s$, respectively. Trends in detonation strength and stability are shown in Fig. 14. For all injector and nozzle configurations, the fundamental frequency of the chamber dynamics increased with $Y_{O_2}^{Ox}$. Tests with Injector A at low T_3 exhibited a narrow range of oxygen content that supported stable, detonative operation, shown in Fig. 14 by the peak in P'/P_c at $Y_{O_2}^{Ox} = 26\%$ and higher power fraction for tests with $Y_{O_2}^{Ox} = 26 - 28\%$. These conditions resulted in stable, counter-propagating detonation waves, while higher and lower oxygen content produced

chaotic chamber dynamics, with inconsistent pressure fluctuation amplitudes and waveforms. At the higher oxidizer inlet temperature range, the range of oxygen contents that produced stable, counter-propagating waves shifted to pure air, $Y_{O_2}^{Ox} = 23.2\%$. While increasing the oxygen content to 26% resulted in low pressure fluctuation amplitude and power fraction characteristic of muddled chamber dynamics, further increases permitted stable combustion fronts to re-form. This is observed in the increase in both P'/P_c and power fraction in Fig. 14.

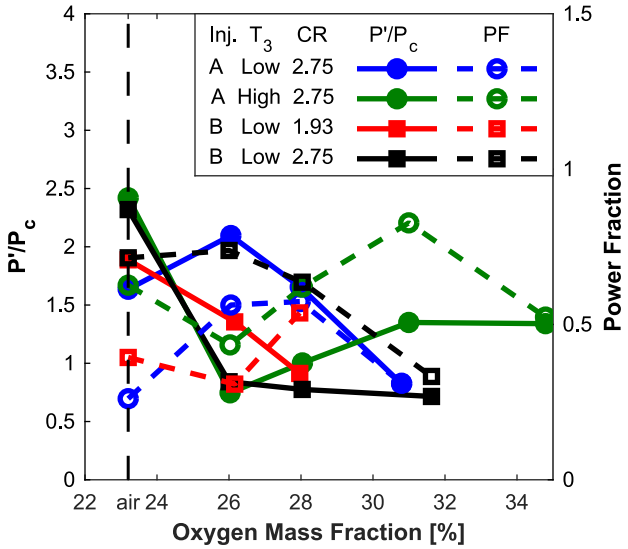

Fig. 14 Sensitivity of combustor operability with respect to mass fraction of oxygen in oxidizer flow, $Y_{O_2}^{Ox}$.

While the addition of oxygen improves detonation stability for injector A at some operating conditions, it appears to uniformly decrease the operational stability for injector B. This is shown by the monotonic decrease in pressure fluctuation amplitude with increasing oxygen content for both nozzle configurations. While the power fraction similarly decreases for the CR = 2.75 nozzle, it increases for the CR = 1.93 nozzle. This is not consistent with observations of raw pressure-time histories and imaging of chamber wave dynamics, illustrating the importance of considering multiple metrics in evaluating combustor operation.

For injector A, the shift in the oxidizer oxygen content that causes the combustor to transition from two to multiple counter-propogating waves at different oxidizer inlet temperatures could be explained by the role of the two parameters in the chemical kinetics of the reactant mixture. RDWC operation requires a fine balance between transient propellant mixing and chemical reaction timescales to present an appropriately prepared mixture to the detonation wave without producing deflagration [41, 45]. Increasing the inlet air temperature or the mass fraction of oxygen are both expected to change the reaction timescales by reducing the ignition delay time of the propellant mixture. Therefore, increasing mixture temperature would require a corresponding decrease in oxygen content to maintain the balance between mixing and chemical kinetics to support detonation in a particular operating regime.

Figure 15 presents the variation in combustor operability with respect to equivalence ratio, conducted with a mass

flux of $250 kg/m^2/s$ and pure air as the oxidizer. The tests with injector A were conducted at the high T_3 condition, while those with injector B used air inlet temperatures in the low range. Both injector configurations produce the strongest, most stable detonation waves at unity equivalence ratio when operating with the CR = 2.75 nozzle. This is seen by the sharp drop in power fraction and pressure fluctuation amplitude moving to fuel-rich or fuel-lean mixtures. In contrast, injector B with the CR = 1.93 nozzle exhibits more stable operation with higher pressure fluctuation amplitudes at lean equivalence ratios. While P'/P_c peaks at $\phi = 0.9$, the power fraction plateaus between $\phi = 0.9 - 0.95$. In particular, the condition with $\phi = 0.9$ produces a single detonation wave in the chamber, while all other conditions result in counter-propagating detonations or steady combustion with no wave fronts visible in high speed imaging.

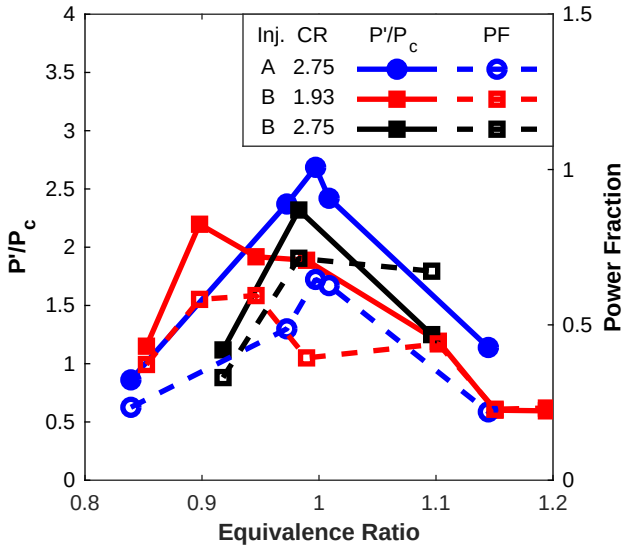

Fig. 15 Sensitivity of combustor operability with respect to equivalence ratio, ϕ. Injector B with the CR = 1.93 nozzle at $\phi = 0.9$ results in operation with a single detonation wave.

Viewing the sensitivities presented in Figs. 14 and 15 together then presents a more complete view of the dependence of combustor operation on the chemical kinetic sensitivity of the propellant mixture. For injector A, the chemical kinetic timescales need to be modestly reduced via enriching the air with oxygen or operating with higher inlet temperatures before a stable, high-amplitude detonation forms. More significant perturbations from further sensitizing the mixture with additional oxygen or departure from the stoichiometric condition significantly diminishes the ability of the detonation to propagate. Injector B with the CR = 2.75 nozzle functions similarly, though unlike injector A does not require the additional sensitization from oxygen or increased air inlet temperature to produce strong, stable detonation waves. The primary difference between these two configurations is the geometry of the injection and mixing regions. The operational differences between the two inlets, where injector A requires enrichment to produce stable detonation waves while injector B does not, could then be attributed to their relative mixing effectiveness and would indicate that injector B better mixes the propellants than injector A. Further enhancing the chemical kinetics with injector B then

produces deflagration burning, as the mixture is able to ignite prior to arrival of subsequent waves.

The same reasoning suggests that injector B with the CR = 1.93 nozzle produces even better mixing. While operation with pure air in the low temperature range produces strong detonations, reducing the equivalence ratio increases the detonation stability, resulting in the bias towards fuel-lean mixtures seen in Fig. 15. The conclusion that reducing the nozzle contraction ratio produces better mixing is consistent with basic fluid dynamics analysis, where decreasing the nozzle contraction ratio increases the pressure ratio across both the fuel and oxidizer injectors. The shock trains within each injectant flow are then stronger and the resultant unsteady interactions result in more complete mixing on shorter spatial/temporal timescales. In addition, the manifolds are better able to re-initiate flow after being checked off by the overpressure from the passing detonation wave. However, this configuration is also observed to produce higher losses [46].

The final operational parameter varied was the mass fraction of hydrogen in the fuel, shown in Fig. 16. A limitation of this study was that the hydrogen could not be premixed with the natural gas and was instead injected via the inner injector of configuration A, while natural gas was flowed through the outer injector. These tests were conducted with $G = 250 kg/m^2/s$, pure air as the oxidizer, $\phi \approx 1$, and T_3 in the range of $710 - 750 K$. Addition of hydrogen resulted in a sharp decrease in the pressure fluctuation amplitude, while the power fraction remained approximately constant across the series of conditions. Inspection of high speed video for tests with hydrogen revealed no wave motion, while individual pressure-time histories exhibited chamber dynamics more similar to combustion instability with smooth, nearly sinusoidal waveforms that produced a high power fraction.

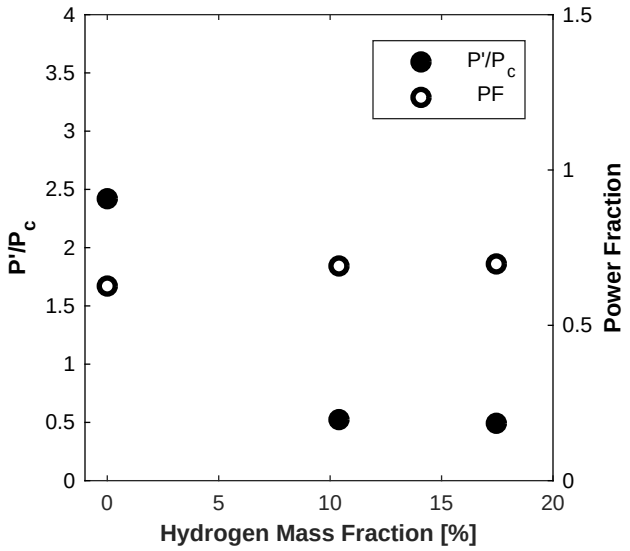

Fig. 16 Sensitivity of combustor operability with respect to hydrogen addition to fuel, $Y^F_{H_2}$, with injector A and nozzle CR = 2.75.

The detonation wave dynamics with hydrogen addition observed in this study do not match trends found in prior

research, where it has been shown to improve detonation strength and stability. Several possible explanations include differences in injection geometry or operating conditions and chemical kinetic limitations. Injection of pure hydrogen from the inner fuel manifold and natural gas from the outer fuel manifold of injector design A is expected to produce radial fuel stratification. As a consequence, a propellant mixture near the inside diameter of the combustor would be more susceptible to deflagration burning, and could interfere with the development of coherent chamber dynamics. Compared to other experiments that have investigated RDWC operation with mixtures of hydrogen and natural gas or methane, this experiment operated at higher air inlet temperatures [13], and higher pressures and natural gas content [16]. Furthermore, at comparable hydrogen mass fractions, $Y_{H_2}^F$, Bykovskii *et al.* observed either poor, unstable detonations or combustion external to the chamber [13]. The tests conducted in this study and by Bykovskii *et al.* could be near a crossover point in the chemical kinetics of hydrogen-natural gas mixtures, where one fuel begins to have a greater effect than the other. Detailed calculations of the chemical kinetics of hydrogen-air mixtures applied to RDWC systems have shown similar crossover points due to pressure variation [45]. The sensitivity to mixture chemical kinetic timescales observed through changing the propellant combination and by variation of equivalence ratio and oxygen addition highlights the importance of testing RDWCs at application relevant flow conditions with corresponding propellants.

IV. Conclusion

Detonation wave dynamics in a high pressure, natural gas-air RDWC were investigated using high frequency pressure measurements and direct imaging of wave motion in the combustor annulus. A broad parametric survey characterized the sensitivity of combustor operability to the mass flux of reactants, oxygen mass fraction in the oxidizer flow, equivalence ratio, and mass fraction of hydrogen in the fuel. Sensitivities were evaluated using pressure fluctuation amplitude as a measure of detonation strength and the fraction of spectral power associated with the primary chamber dynamics, termed the power fraction, for comparison of operational mode stability.

Global evaluation of detonation quality showed that combustion fronts in the combustor propagate at a minimum velocity of approximately 50% of the mixture CJ detonation velocity. This could correspond to a precursor shock-turbulent flame complex that forms a CJ deflagration wave. Comparing operability metrics to the estimated detonation cell size for each test showed that cell size should be at most of the order of the chamber gap, but that smaller cell sizes fail to guarantee formation of high-order detonation waves. This supports the view of the cell size as an approximate scaling parameter for RDWC design, due to the non-canonical flow and boundary conditions found in a combustor.

Comparison of combustor operation at different mass fluxes showed that higher chamber pressures likely suppressed the detonation, resulting weaker pressure fluctuation amplitudes and less stable wave propagation for the studied configurations. Parametric variation of the oxidizer oxygen content showed that injector A required limited sensitization to support robust detonation, but that further oxygen enrichment resulted in more waves and chaotic pressure-time histories. Increasing the oxidizer inlet temperature reduced the range of oxygen content that supported stable operation

to pure air, pointing to changes in chemical kinetics as an important factor. In comparison, injector B required no sensitization with the CR = 2.75 backpressure nozzle, and produced stronger detonation waves at fuel-lean conditions with the CR = 1.93 nozzle. This suggests that injector B produces better mixing than injector A, as any method of sensitizing the mixture results in less coherent chamber dynamics or steady deflagration. Finally, addition of hydrogen to the fuel was shown to result in deflagrative combustion with no wave motion.

The parametric survey showed that chamber wave dynamics are typically characterized by multiple, counter-rotating detonation heads. However, a limited range of conditions with injector B and the CR = 1.93 nozzle exhibited sustained operation with a single detonation wave. To the authors' knowledge, this is the first demonstration of RDWC operation with a single wave using natural gas and air as propellants.

V. Acknowledgements

This research was supported by the University Turbine Systems Research program under contract DE-FE0025343, with contract monitor Mark Freeman. The authors are also grateful to Scott Meyer, for his critical guidance in the development of the experiment, and to Robert McGuire, for his tireless assistance.

References

[1] Paxson, D. E., and Kaemming, T., "Influence of Unsteadiness on the Analysis of Pressure Gain Combustion Devices," *Journal of Propulsion and Power*, Vol. 30, No. 2, 2014, pp. 377–383. doi:10.2514/1.b34913.

[2] Nordeen, C. A., "Thermodynamics of a Rotating Detonation Engine," Doctoral dissertation, University of Connecticut, 2013.

[3] Lu, F. K., and Braun, E. M., "Rotating Detonation Wave Propulsion: Experimental Challenges, Modeling, and Engine Concepts," *Journal of Propulsion and Power*, Vol. 30, No. 5, 2014, pp. 1125–1142. doi:10.2514/1.b34802.

[4] Rankin, B. A., Richardson, D. R., Caswell, A. W., Naples, A. G., Hoke, J. L., and Schauer, F. R., "Chemiluminescence imaging of an optically accessible non-premixed rotating detonation engine," *Combustion and Flame*, Vol. 176, 2017, pp. 12–22. doi:10.1016/j.combustflame.2016.09.020.

[5] Stechmann, D. P., "Experimental Study of High-Pressure Rotating Detonation Combustion in Rocket Environments," Doctoral dissertation, Purdue University, 2017.

[6] Kailasanath, K., and Schwer, D. A., "High-fidelity simulations of pressure-gain combustion devices based on detonations," *Journal of Propulsion and Power*, Vol. 33, No. 1, 2017, pp. 153–162. doi:10.2514/1.B36169.

[7] Bykovskii, F. A., Zhdan, S. A., and Vedernikov, E. F., "Continuous Spin Detonations," *Journal of Propulsion and Power*, Vol. 22, No. 6, 2006, pp. 1204–1216. doi:10.2514/1.17656.

[8] Bohon, M. D., Bluemner, R., Paschereit, C. O., and Gutmark, E. J., "High-speed imaging of wave modes in an RDC," *Experimental Thermal and Fluid Science*, Vol. 102, No. August 2018, 2019, pp. 28–37. doi:10.1016/j.expthermflusci.2018.10.031.

[9] Fotia, M. L., Hoke, J., and Schauer, F., "Experimental Performance Scaling of Rotating Detonation Engines Operated on Gaseous Fuels," *Journal of Propulsion and Power*, Vol. 33, No. 5, 2017, pp. 1–10. doi:10.2514/1.B36213.

[10] Bennewitz, J. W., Bigler, B. R., Pilgram, J. J., and Hargus, Jr., W. A., "Modal Transitions in Rotating Detonation Rocket Engines," *International Journal of Energetic Materials and Chemical Propulsion*, Vol. 18, No. 2, 2019, pp. 91–109. doi:10.1615/intjenergeticmaterialschemprop.2019027880.

[11] Tobias, J., Depperschmidt, D., Welch, C., Miller, R., Uddi, M., Agrawal, A. K., and Daniel, R., "OH* Chemiluminescence Imaging of the Combustion Products From a Methane-Fueled Rotating Detonation Engine," *Journal of Engineering for Gas Turbines and Power*, Vol. 141, No. 2, 2019, pp. 1–11. doi:10.1115/1.4041143.

[12] Bykovskii, F. A., Zhdan, S. A., Vedernikov, E. F., and Samsonov, A. N., "Scaling factor in continuous spin detonation of syngas–air mixtures," *Combustion, Explosion, and Shock Waves*, Vol. 53, No. 2, 2017, pp. 187–198. doi:10.1134/S0010508217020095.

[13] Bykovskii, F. A., Zhdan, S. A., and Vedernikov, E. F., "Continuous Detonation of Methane/Hydrogen–Air Mixtures in an Annular Cylindrical Combustor," *Combustion, Explosion, and Shock Waves*, Vol. 54, No. 4, 2018, pp. 472–481. doi: 10.1134/s0010508218040111.

[14] Bykovskii, F. A., and Zhdan, S. A., "Continuous spin detonation of poorly detonable fuel-air mixtures in annular combustors," *Journal of Physics: Conference Series*, Vol. 899, No. 4, 2017, pp. 1–7. doi:10.1088/1742-6596/899/4/042002.

[15] Roy, A., Ferguson, D. H., Sidwell, T., O'Meara, B., Strakey, P., Bedick, C., and Sisler, A., "Experimental Study of Rotating Detonation Combustor Performance under Preheat and Back Pressure Operation," AIAA 2017-1065, 2017. doi: 10.2514/6.2017-1065.

[16] Roy, A., Ferguson, D., Sidwell, T., and Strakey, P., "Characteristics of a Non-Premixed Rotating Detonation Combustor Using Natural Gas-Hydrogen Blend at Elevated Air-Preheat Temperature and Backpressure," *IMECE*, 2018. doi:10.1115/imece2018-88569.

[17] Meyer, S. E., Heister, S. D., Slabaugh, C., Lucht, R. P., Pratt, A., Gejji, R. M., Bedard, M., and Lemcherfi, A., "Design and Development of the High Pressure Combustion Laboratory at Purdue University," AIAA 2017-4965, 2017. doi: 10.2514/6.2017-4965.

[18] Slabaugh, C. D., Pratt, A. C., Lucht, R. P., Meyer, S. E., Benjamin, M., Lyle, K., and Kelsey, M., "The development of an optically accessible, high-power combustion test rig," *Review of Scientific Instruments*, Vol. 85, No. 3, 2014. doi:10.1063/1.4867084.

[19] Vectern Energy Delivery, "Tuscola East Mainline PEPL Daily Average Gas Quality Info," , 2017. URL `https://peplmessenger.energytransfer.com`.

[20] European Committee for Standardization, "ISO 9300: Measurement of gas flow by means of critical flow," International Organization for Standardization, 2005.

[21] Lemmon, E., Huber, M., and McLinden, M., "NIST Reference Fluid Thermodynamic and Transport Properties (REFPROP), Version 9.3 - SRD 23," National Institute of Standards and Technology, 2018. doi:10.18434/T4JS3C.

[22] Kline, S., and McClintock, F., "Describing Uncertainties in Single-Sample Experiments," *Mechanical Engineering*, Vol. 75, No. January, 1953, pp. 3–8.

[23] Miller, S. J., "Design and Testing of an H2/O2 Predetonator for a Simulated Rotating Detonation Engine Channel," Masters thesis, Air Force Institute of Technology, 2013.

[24] St. George, A., Driscoll, R., Anand, V., and Gutmark, E., "On the existence and multiplicity of rotating detonations," *Proceedings of the Combustion Institute*, Vol. 36, No. 2, 2017, pp. 2691–2698. doi:10.1016/j.proci.2016.06.132.

[25] Radulescu, M. I., Sharpe, G. J., Law, C. K., and Lee, J. H., "The hydrodynamic structure of unstable cellular detonations," *Journal of Fluid Mechanics*, Vol. 580, No. June, 2007, pp. 31–81. doi:10.1017/S0022112007005046.

[26] Lee, J. H., *The Detonation Phenomenon*, 1st ed., Cambridge University Press, Cambridge, 2008. doi:10.1017/CBO9780511754708.

[27] Kaneshige, M., and Shepherd, J., "Detonation Database," Technical Report FM97-8, GALCIT, 1997.

[28] Stevens, C. A., Hoke, J., and Schauer, F., "Propane-Air Cell Size Correlation to Temperature and Pressure," AIAA 2016-1400, 2016. doi:10.2514/6.2016-1400.

[29] Bauer, P. A., Presles, H. N., Heuze, O., and Brochet, C., "Measurement of cell lengths in the detonation front of hydrocarbon oxygen and nitrogen mixtures at elevated initial pressures," *Combustion and Flame*, Vol. 64, No. 1, 1986, pp. 113–123. doi:10.1016/0010-2180(86)90102-1.

[30] Siwiec, S., and Wolańskl, P., "Detonation cell structure in CH4-air mixture at high pressure," *Archivum Combustionis*, Vol. 4, No. 3, 1984, pp. 249–252.

[31] Westbrook, C. K., "Chemical Kinetics of Hydrocarbon Oxidation in Gaseous Detonations," *Combustion and Flame*, Vol. 46, 1982, pp. 191–210. doi:10.2514/5.9781600865695.0151.0174.

[32] Westbrook, C. K., and Haselman, L. C., "Chemical Kinetics in LNG Detonations," *Gasdynamics of Detonations and Explosions*, edited by A. Oppenheim, N. Manson, R. Soloukhin, and J. Bowen, AIAA, 1980, pp. 193–206. doi:10.2514/5.9781600865497.0193.0206.

[33] Katta, V. R., Cho, K. Y., Hoke, J. L., Codoni, J. R., Schauer, F. R., and Roquemore, W. M., "Effect of increasing channel width on the structure of rotating detonation wave," *Proceedings of the Combustion Institute*, Vol. 000, 2018, pp. 1–9. doi:10.1016/j.proci.2018.05.072.

[34] Frolov, S. M., Aksenov, V. S., Ivanov, V. S., and Shamshin, I. O., "Large-scale hydrogen-air continuous detonation combustor," *International Journal of Hydrogen Energy*, Vol. 40, No. 3, 2015, pp. 1616–1623. doi:10.1016/j.ijhydene.2014.11.112.

[35] Sun, J., Zhou, J., Liu, S., Lin, Z., and Lin, W., "Effects of air injection throat width on a non-premixed rotating detonation engine," *Acta Astronautica*, Vol. 159, 2019, pp. 189–198. doi:10.1016/j.actaastro.2019.03.067.

[36] Walters, I. V., Journell, C., Lemcherfi, A., Gejji, R., Heister, S. D., and Slabaugh, C. D., "Experimental Investigation of a Piloted, Natural Gas-Air Rotating Detonation Wave Combustor," AIAA 2018-4782, 2018. doi:10.2514/6.2018-4782.

[37] Bykovskii, F. A., Zhdan, S. A., Vedernikov, E. F., Samsonov, A. N., Sychev, A. I., and Tarnaikin, A. E., "Pressure measurement by fast-response piezo-electric sensors during continuous spin detonation in the combustor," *Combustion, Explosion, and Shock Waves*, Vol. 53, No. 1, 2017, pp. 65–73. doi:10.1134/S0010508217010105.

[38] Gejji, R. M., Walters, I. V., Lemcherfi, A., Sardeshmukh, S. V., Heister, S. D., and Slabaugh, C. D., "Transducer Installation Effects on Pressure Measurements in PGC Devices," AIAA 2018-0158, 2018. doi:10.2514/6.2018-0158.

[39] Bennewitz, J. W., Bigler, B. R., Schumaker, S. A., and Hargus, W. A., "Automated image processing method to quantify rotating detonation wave behavior," *Review of Scientific Instruments*, Vol. 90, No. 6, 2019, pp. 1–12. doi:10.1063/1.5067256.

[40] Walters, I. V., Journell, C. L., Lemcherfi, A., Gejji, R., Heister, S. D., and Slabaugh, C. D., "Parametric Survey of a Natural Gas-Air Rotating Detonation Engine at Elevated Pressure," AIAA 2019-1510, 2019. doi:10.2514/6.2019-1510.

[41] Schwinn, K., Gejji, R., Kan, B., Sardeshmukh, S., Heister, S., and Slabaugh, C. D., "Self-sustained, high-frequency detonation wave generation in a semi-bounded channel," *Combustion and Flame*, Vol. 193, 2018, pp. 384–396. doi: 10.1016/j.combustflame.2018.03.022.

[42] Pincus, S., "Approximate entropy (ApEn) as a complexity measure," *Chaos*, Vol. 5, No. 1, 1995, pp. 110–117. doi: 10.1063/1.166092.

[43] Chue, R., Clarke, J., and Lee, J. H., "Chapman-Jouguet Deflagrations," *Proceedings: Mathematical and Physical Sciences*, Vol. 441, No. 1913, 1993, pp. 607–623. doi:10.1098/rspa.1993.0082.

[44] Paxson, D. E., and Schwer, D. A., "Operational Stability Limits in Rotating Detonation Engine Numerical Simulations," AIAA 2019-0748, 2019. doi:10.2514/6.2019-0748.

[45] Stechmann, D. P., Sardeshmukh, S., Heister, S. D., and Mikoshiba, K., "Role of Ignition Delay in Rotating Detonation Engine Performance and Operability," *Journal of Propulsion and Power*, Vol. 35, No. 1, 2018, pp. 125–140. doi:10.2514/1.b37117.

[46] Kaemming, T., Fotia, M. L., Hoke, J., and Schauer, F., "Thermodynamic Modeling of a Rotating Detonation Engine Through a Reduced-Order Approach," *Journal of Propulsion and Power*, Vol. 33, No. 5, 2017, pp. 1170–1178. doi:10.2514/1.b36237.